Calculation of ground state rotational populations for kinetic gas homonuclear diatomic molecules including electron-impact excitation and wall collisions

David R. Farley

Citation: J. Chem. Phys. **133**, 094303 (2010); doi: 10.1063/1.3475000
View online: http://dx.doi.org/10.1063/1.3475000
View Table of Contents: http://jcp.aip.org/resource/1/JCPSA6/v133/i9
Published by the American Institute of Physics.

Calculation of ground state rotational populations for kinetic gas homonuclear diatomic molecules including electron-impact excitation and wall collisions

David R. Farley[a)]
Princeton Plasma Physics Laboratory, Princeton, New Jersey 08543, USA

(Received 2 March 2010; accepted 14 July 2010; published online 3 September 2010)

A model has been developed to calculate the ground state rotational populations of homonuclear diatomic molecules in kinetic gases, including the effects of electron-impact excitation, wall collisions, and gas feed rate. The equations are exact within the accuracy of the cross sections used and of the assumed equilibrating effect of wall collisions. It is found that the inflow of feed gas and equilibrating wall collisions can significantly affect the rotational distribution in competition with nonequilibrating electron-impact effects. The resulting steady-state rotational distributions are generally Boltzmann for $N \geq 3$, with a rotational temperature between the wall and feed gas temperatures. The $N=0,1,2$ rotational level populations depend sensitively on the relative rates of electron-impact excitation versus wall collision and gas feed rates. © *2010 American Institute of Physics*. [doi:10.1063/1.3475000]

I. INTRODUCTION

Rotational temperature estimates obtained from measured spectra may often be correlated with the neutral gas translational temperature since rotational and translational modes for most small molecules typically equilibrate within 3–20 intermolecular collisions.[1] This assumes that the gas and experiment conditions justify even this number of collisions occurring prior to any other nonequilibrating interactions, such as electron-impact excitation collisions. Otherwise the rotational modes cannot necessarily be assumed to be in equilibrium with the translational modes, and no direct connection between rotational temperature and gas temperature can be made. Additionally, hydrogen requires an abnormally large number of intermolecular collisions (~300) for rotational and translational modes to equilibrate at normal temperatures (~200 for deuterium).[2,3] Therefore, intermolecular collisions are not as effective at equilibrating internal energy modes of hydrogen, and other mechanisms must be studied to quantify the rotational level populations.

As described by Otorbaev,[4] there has been considerable debate as to the ground state rotational distribution of hydrogen. Multiple studies on electron-impact excitation of hydrogen have reported non-Boltzmann distributions and purported various explanations.[5–12] In particular, Lavrov *et al.*[9] developed a rotational distribution model using detailed balancing with intermolecular collisions and quadrupole electron-impact excitation of ground state rotational levels. However, Lavrov *et al.* were apparently unaware that intermolecular collisions are rather ineffective at equilibrating rotational modes. Also, their recursive formula for rotational level populations, which is a weighted sum of Boltzmann distributions corresponding to a gas temperature and an electron temperature, is not applicable for electron energies greater than ~5 eV since this would result in their model predicting inordinately high rotational levels being primarily populated, and hydrogen dissociates at 4.5 eV.

Further, Lavrov *et al.* did not include other processes such as dipole-allowed, bound-electronic rovibrational transitions (so-called vibronic transitions), nor the potentially strong effects of wall collisions and feed gas. These effects will be considered here to create a more complete model to describe the ground state rotational distribution. The model will be applied to the kinetic hydrogen plasma of the Princeton Field-Reversed Configuration (PFRC) device[13] being operated at the Princeton Plasma Physics Laboratory, which has a nominal hydrogen gas density of $n_{H_2} \sim 3 \times 10^{13}$ cm^{-3} and thermal energy of $T_e \sim 100-200$ eV electron distribution at a density of $n_e \sim 10^{12}$ cm^{-3}. Since there is some concern whether measured PFRC rotational spectra follow dipole selection rules allowing a direct comparison of measured rotational lines with ground state populations, no comparison will be made with PFRC data (this will be done in a subsequent publication). The model will be applied to the low-energy gas discharge results of Otorbaev *et al.*[4,5] The methodology described herein could be adapted to other homonuclear molecules and gas dynamic scenarios.

II. THEORY

To create a model for the populations of the rotational levels of the ground electronic state of hydrogen ($X\ ^1\Sigma_g^+$), applicable incoming and outgoing rates for each rotational level are needed. These rates are those due to the addition of equilibrium feed gas, electron-impact excitation, emission, and wall collisions. Intermolecular collisions are not considered due to the hydrogen equilibration issue cited above and can be neglected for kinetic plasmas such as the PFRC or rarefied gas dynamics where wall collisions occur much more frequently than intermolecular collisions. However, in

[a)]Electronic mail: dfarley@pppl.gov.

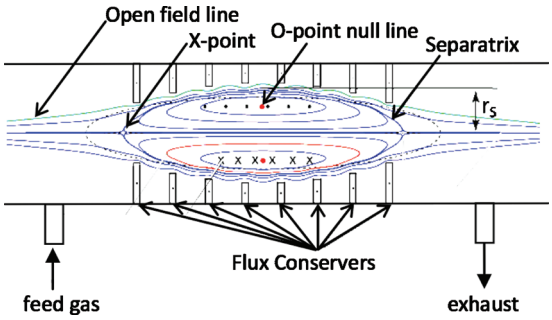

FIG. 1. Schematic of the Princeton Field-Reversed Configuration device at the Princeton Plasma Physics Laboratory. Illustrated (not to scale) are the vacuum chamber, gas feed inlet and exhaust outlet, copper magnetic flux conservers, and magnetic field lines. r_s is the radial distance of the separatrix at the axial centerline.

denser hydrogen gases, where intermolecular collisions are much more frequent, intermolecular equilibration must be considered.

These rates applicable to homonuclear diatomic molecules are described below, using characteristics of the PFRC experiment as an example. A sketch of the PFRC is shown in Fig. 1, including its tantalum-clad copper magnetic flux conserver rings.

The feed gas flow rate is denoted as Γ in standard cubic centimeters per minute (SCCM). At STP, the number density is 2.65×10^{19} cm^{-3}. The inflow of H_2 molecules into the PFRC vacuum chamber is $2.65\times10^{19}\Gamma$ molecules per minute. The volume of the PFRC vacuum chamber is approximately 8000 cm^3, giving a H_2 density influx rate of $3\times10^{15}\Gamma$ molecules/cm^3 min. The incoming H_2 molecules pass through a long length of room temperature piping before entering the PFRC and are assumed to have a Boltzmann rotational distribution at a feed temperature T_{feed}. The rate of population addition to the rotational levels, in units of cm^{-3} s^{-1}, is then given by

$$\dot{n}_N^{\text{feed}} = 2\times10^{17}\Gamma(2N+1) \times\exp\{-BhcN(N+1)/kT_{\text{feed}}\}/Q_{\text{rot}}, \quad (1)$$

where N is the rotational quantum number ($N=0,1,2,\ldots$), B is the rotational constant for hydrogen in its ground state, Q_{rot} is the rotational partition function, h is Planck's constant, c is the speed of light, and k is Boltzmann's constant (Γ is still in units of SCCM). Noting that $Bhc/k=87$ K (Ref. 14) and $Q_{\text{rot}}=kT_{\text{feed}}/2Bhc$,[15] Eq. (1) can be rewritten as

$$\dot{n}_N^{\text{feed}} = 2\times10^{17}\Gamma\frac{174}{T_{\text{feed}}}(2N+1)\exp\{-87N(N+1)/T_{\text{feed}}\}. \quad (2)$$

The PFRC H_2 feed rate is typically $\Gamma=2-4$ SCCM to maintain a 1 mTorr pressure in the vacuum chamber. An effective "excitation" rate of population into the N rotational state can be estimated by dividing the $2\times10^{17}\Gamma$ cm^{-3} s^{-1} of Eq. (2) by the nominal PFRC vacuum chamber H_2 density of 3×10^{13} cm^{-3}. Assuming the feed temperature is at approximately room temperature gives a characteristic rate of approximately 10–20 kHz for the PFRC.

Hydrogen will also flow out of the vacuum chamber at a flow rate equal to the feed rate to maintain a constant chamber density. However, because of their long residence time in the chamber (~1 s), the molecules will have achieved a steady-state rotational distribution by the time they exit the system, so the outflow will not affect the rotational distribution.

Electron-impact can cause transitions among the rotational levels. Homonuclear diatomic molecules such as H_2 are nonpolar and therefore purely rotational or rovibrational radiative dipole transitions are not possible since homonuclear molecules possess no permanent electric dipole moment.[14] Also, such dipole rovibrational transitions are forbidden regardless by molecular symmetry rules when there is no associated bound-electron excitation. It is possible to cause rotational transitions without bound-electron excitation through electric quadrupole radiative transitions, or Raman scattering, but these transitions must cause $\Delta N=0,\pm2$ due both to the nature of the interaction as well as to satisfy symmetry-enforced selection rules. However, electric quadrupole-induced radiative emissions have intensities typically 10^{-9} that of electric dipole emissions,[14] effectively leaving only Raman scattering as an option for rotational spectroscopy through electromagnetic radiation. Electron-impact excitation of ground electronic state molecules, which still must satisfy the $\Delta N=0,\pm2$ selection rule, can cause quadrupole transitions of non-negligible strength, sometimes as high as 10%–20% of dipole transitions in electron-impact of H_2.[16] The rate of excitation out of state N due to quadrupole electron-impact scattering can be estimated through[17–19]

$$\dot{n}_{N\to N+2}^{\text{quad}} = n_N n_e\langle\sigma_{0\to2}V_e\rangle(2N+5)\begin{pmatrix} N+2 & N & 2 \\ 0 & 0 & 0\end{pmatrix}^2, \quad (3)$$

where $\sigma_{0\to2}$ is the electron-impact excitation cross section for purely rotational transitions from $N=0$ to $N=2$, V_e is the electron speed, and the matrix in braces is the Wigner $3-j$ symbol. The $3-j$ symbol squared in Eq. (3) is $3(N+2)\times(N+1)/2(2N+5)(2N+3)(2N+1)$,[20] simplifying Eq. (3) to

$$\dot{n}_{N\to N+2}^{\text{quad}} = n_N n_e\langle\sigma_{0\to2}V_e\rangle\frac{3}{2}\frac{(N+2)(N+1)}{(2N+3)(2N+1)}. \quad (4)$$

Equation (4) gives the rate of population transfer out of state N, but state N will also receive population from the $N-2$ state below it. This amount coming into N from $N-2$ is calculated by replacing N with $N-2$ in Eq. (4). Therefore, the net population rate *into* state N is

$$\dot{n}_N^{\text{quad}} = n_N n_e\langle\sigma_{0\to2}V_e\rangle\frac{3}{2}\left[\frac{N(N-1)}{(2N-1)(2N-3)} - \frac{(N+2)(N+1)}{(2N+3)(2N+1)}\right]. \quad (5)$$

Note that the $N=0$ and $N=1$ rotational states always have a net outflow of population, which is absorbed by the $N\geq2$ levels. Equation (5) is properly normalized such that the total number of particles remains unchanged, i.e., the rotational populations are simply adjusted among rotational states with

each electron-impact. The reverse direction of quadrupole electron-impact excitation ($N \rightarrow N-2$) can also be calculated,[19] where it is found that the cross section for these transitions is about 2% of $\sigma_{N\rightarrow N+2}$. These reverse transitions are therefore not included here.

Vibrational quadrupole transitions are also possible for nonpolar molecules such as H_2. However, the probability of transition from the ground $v=0$ to excited $v'=1$ vibrational states is $<3\%$ of remaining within the (0,0) band.[21] Higher vibrational changes are even less likely. Therefore, quadrupole vibrational transitions will be neglected.

The cross section for quadrupole rotational excitation of hydrogen impacted by ~ 100 eV electrons ($V_e=4.2\times 10^8$ cm/s) is $\sigma_{0\rightarrow 2}\cong 9\times 10^{-18}$ cm^2.[22,23] However, the 100 eV electrons are mainly confined to the region within the magnetic flux conservers of the PFRC, as depicted in Fig. 1, which have a characteristic inner diameter of 7 cm, whereas the vacuum chamber diameter is 10 cm. Therefore, the probability of excitation should be reduced by the relative areas $(7/10)^2$. For situations where electrons are not confined within a subsection of the vacuum chamber, this factor can of course be neglected. Putting these values into Eq. (5) results in a characteristic excitation rate due to quadrupole electron-impact transitions of ~ 3 kHz for the PFRC.

In the case of electron-impact scattering causing rovibronic excitation, where bound-electron transitions occur as well as rotational transitions, nonpolar molecules such as H_2 do have dipole spectra, in contrast with purely rotational or rovibrational transitions discussed above. Scattering events occur which maintain the total spin of the term, or can cause spin-exchange transitions whereby otherwise spin-enforced forbidden transitions are then allowed. In the case of the singlet ground electronic state $X\ ^1\Sigma_g^+$ of H_2, transitions to triplet electronic states, which are forbidden for radiative transitions, do occur through electron-impact excitation. However, the excited triplets decay eventually to the repulsive b $^3\Sigma_u^+$ electronic state, which then results in dissociation of the molecule. Spin-exchange electronic transitions thereby remove those triplet-H_2 molecules from the sea of singlet molecules, and thus only the singlet-singlet electronic excitations can have an effect on the ground state rotational distribution upon their decay back to the ground electronic state. In other words, singlet to triplet excitations may result in dissociation of the molecules affected, but will not alter the rotational population distribution of remaining molecules in the ground singlet electronic state.

In contrast with purely rotational and rovibrational quadrupole excitations where populations transfer primarily only toward increasing N, rovibronic transitions can populate upward rotational levels as well as backward. This is illustrated in the Fig. 2 "bucket diagram" depicting both the $^1\Sigma$-$^1\Sigma$ [Fig. 2(a)] and $^1\Sigma$-$^1\Pi$ electronic transitions [Fig. 2(b)]. In Fig. 2, focus is put on the $N=2$ ground rotational state (N' refers to upper rotational states) to avoid clutter in depicting all transitions. For Σ-Σ electronic transitions ($\Delta\Lambda=0$, where Λ is the projection of total bound-electron angular momentum on the internuclear axis), $\Delta N=0$ is not allowed and therefore there can be no Q-branch transitions. Electron-impact dipole excitation is denoted by solid arrows and dipole radiative

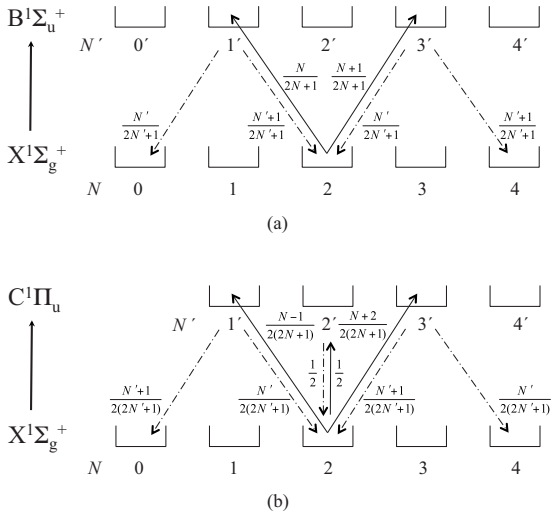

FIG. 2. Illustration of electron-impact dipole excitation and radiative dipole emission of the H_2 $X\ ^1\Sigma_g^+$ ground state for bound-electron singlet-singlet transitions. (a) Excitation to a higher-level $^1\Sigma$ electronic state (Q-branches not allowed) and (b) excitation to a $^1\Pi$ electronic state (which has no $N=0$ rotational state).

emission with dot-dash arrows. As can be seen in Fig. 2(a), a Σ-Σ rotational level will have four contributions to its population: two dipole excitations out and two dipole emissions in. The rate of these dipole transitions can be calculated with appropriate dipole $3-j$ symbols, or equivalently so-called Hönl–London factors.[14,24] These Hönl–London factors are listed next to the associated transition arrows in Fig. 2, normalized to sum to unity such that the factors listed are the relative probabilities for excitation or emission. Notice that emission backward to lesser N is possible in rovibronic transitions, such that this process can be thought of as a reshuffling of the rotational level populations.

It is assumed that equal amounts of population from each rotational level are excited by electron-impact. Justification derives from the Born–Oppenheimer approximation[25] which allows the separation of electronic modes from rovibrational modes by assuming nuclear motion is essentially frozen during the electron scattering process. Therefore, bound-electron excitation is independent of the rovibrational states in this approximation.

Most excited populations decay back into the $X\ ^1\Sigma_g^+$ ground electronic state, except for those from the $B'\ ^1\Sigma_u^+$ electronic state, a part of which decay into the metastable $EF\ ^1\Sigma_g^+$ state.[26] The rotational population changes due to cascade transitions from the $I\ ^1\Pi_g$, $J\ ^1\Delta_g$, and $H\bar{H}\ ^1\Sigma_g^+$ higher electronic states will not be considered, assuming their contribution to the rotational levels is small in comparison with the rate of direct transitions. The allowed upper singlet electronic states with highest cross section are the $B\ ^1\Sigma_u^+$ and $C\ ^1\Pi_u$ states, having cross sections of 3×10^{-17} cm^2 for 100 eV electron-impact excitation.[27] Although of lower cross section by nearly an order of magnitude (see Table I),[27] the $B'\ ^1\Sigma_u^+$, $B''\ ^1\Sigma_u^+$, $D\ ^1\Pi_u$, and $D'\ ^1\Pi_u$ electronic states add to the overall excitation rate, so those will be included.

Additionally, vibrational transitions of non-negligible probability occur during electron-impact excitation of electronic states and subsequent emission, following the Franck–

TABLE I. Electron-impact cross sections σ from the X $^1\Sigma_g^+$ ground electronic state for different upper electronic states (Ref. 27) and fraction f of excited population returning to vibrational $v=0$ ground state.

	Upper electronic state					
	B $^1\Sigma_u^+$	B′ $^1\Sigma_u^+$	B″ $^1\Sigma_u^+$	C $^1\Pi_u$	D $^1\Pi_u$	D′ $^1\Pi_u$
$\sigma(\times 10^{-18}$ cm$^2)$	30	4	1.5	30	3	2
f	0.025	0.040	0.055	0.097	0.087	0.084

Condon approximation, which has been shown to hold for H_2.[28,29] Since the ground state of hydrogen is being considered here, the net amount of population returning to the ground vibrational state $v=0$ must be considered. The vibrational populations are assumed to be Boltzmann following the distribution $n_v=n_{H_2}e^{-G(v)/T_{vib}}/Q_{vib}$, where $G(v)=4,395.2(v+1/2)-117.99(v+1/2)^2$ is the vibrational energy (in units of cm^{-1}),[14] T_{vib} is the distribution's vibrational temperature, and Q_{vib} is the vibrational partition function. Separate analysis of vibrational bands of measured PFRC spectra[30] has shown that the PFRC has a Boltzmann vibrational distribution with a vibrational temperature between 5000 and 6000 K. The vibrational population excited from lower states v to upper states v' is calculated using Franck–Condon factors $q_v^{v'}$ through $n_{v'}=n_{H_2}\Sigma_v q_v^{v'}e^{-G(v)/T_{vib}}/Q_{vib}$. The fraction f of excited population returning to the ground vibrational state is $\Sigma_{v'}n_{v'}q_{v=0}^{v'}$. Thus, the fraction of population returning to the ground vibrational state is given by $f=\Sigma_{v'}q_{v=0}^{v'}\Sigma_v q_v^{v'}e^{-G(v)/T_{vib}}/Q_{vib}$. Fractions were calculated for all the electronic transitions considered, as detailed in Table I, which changed very little ($<1\%$) from room temperature to 9000 K. Franck–Condon factors of Fantz and Wünderlich[26] were used, including upper state vibrational states as high as $v'=36$. These factors can be incorporated into the excitation rate by multiplying the factor f by the relevant electron-impact cross section for each electronic transition.

With the above assumptions and appropriate Hönl–London factors ($3-j$ symbols for dipole transitions), the net population rate into rotational state N due to allowed X $^1\Sigma_g^+\leftrightarrow$B $^1\Sigma_u^+$ and X $^1\Sigma_g^+\leftrightarrow$C,D $^1\Pi_u$ rovibronic transitions, respectively, are

$$\dot{n}_N^{\Sigma\leftrightarrow\Sigma}=n_N n_e\sum_{B,B',B''}f_i\langle\sigma_i V_e\rangle\left[\frac{N+1}{2N+3}\left(\frac{N+1}{2N+1}+\frac{N+2}{2N+5}\right)+\frac{N}{2N-1}\left(\frac{N-1}{2N-3}+\frac{N}{2N+1}\right)-1\right], \tag{6a}$$

$$\dot{n}_N^{\Sigma\leftrightarrow\Pi}=n_N n_e\sum_{C,D,D'}f_i\langle\sigma_i V_e\rangle\left[\frac{N-1}{2(2N-1)}\left(\frac{N}{2(2N-3)}+\frac{1}{2}+\frac{N-1}{2(2N+1)}\right)+\frac{1}{2}\left(\frac{N+1}{2(2N-1)}+\frac{1}{2}+\frac{N}{2(2N+3)}\right)+\frac{N+2}{2(2N+3)}\left(\frac{N+2}{2(2N+1)}+\frac{1}{2}+\frac{N+1}{2(2N+5)}\right)-1\right]. \tag{6b}$$

The summation is over the relevant electronic transitions: X $^1\Sigma_g^+\rightarrow$B $^1\Sigma_u^+$, B′ $^1\Sigma_u^+$, and B″ $^1\Sigma_u^+$ for Eq. (6a), and X $^1\Sigma_g^+\rightarrow$C $^1\Pi_u$, D $^1\Pi_u$, and D′ $^1\Pi_u$ for Eq. (6b). Note that the electron-impact excitation cross sections have a threshold of ~14 eV, so low-energy discharges should not include these rovibronic excitation contributions in the model.

Equation (6) must also be multiplied by the magnetic flux conserver to vacuum chamber cross-sectional areas as described prior, if appropriate. For $\Sigma\leftrightarrow\Sigma$ transitions, both the $N=0$ and $N=1$ levels will always have net outflow of population, whereas for $\Sigma\leftrightarrow\Pi$ transitions only the $N=0$ level is always losing population. Using the above cross sections for the relevant bound-electronic transitions, the characteristic excitation frequency for rovibronic transitions into state N is ~0.2–0.6 kHz in the PFRC. This rate is much lower than that for quadrupole electron-impact excitation (~3 kHz) or the gas feed rate (10–20 kHz), but will regardless be included in the analysis.

The thermal velocity of H_2 molecules in the PFRC is $V_{H_2}=9.8\times10^5(T_{gas}/23\ 210\ \text{K})^{1/2}$ cm/s,[31] which for the PFRC temperatures of 300–1000K corresponds to velocities of $1-2\times10^5$ cm/s. The PFRC vacuum chamber diameter is $D=10$ cm, resulting in a wall collision frequency of $V_{H_2}/D=10-20$ kHz. Equilibration of the wall temperature with rotational modes occurs over several wall collisions.[32] It is assumed that the rotational populations linearly approach a Boltzmann distribution with each wall collision, denoting ζ as the fraction of molecules achieving equilibrium with the wall in one collision. The rate of rotational population change is then

$$\begin{aligned}\dot{n}_N^{wall}&=\frac{V_{H_2}}{D}\cdot\zeta\{n_{H2}(2N+1)\exp[-BhcN(N+1)/kT_{wall}]/Q_{rot}-n_N\}\\&=\frac{6.4\times10^3\zeta\sqrt{T_{gas}}}{D}\cdot\{n_{H2}(174K/T_{wall})(2N+1)\times\exp[-87N(N+1)/T_{wall}]-n_N\},\end{aligned} \tag{7}$$

where T_{gas} is in degrees Kelvin and the population rate in units of cm^{-3} s^{-1}. ζ can be calculated from the number of collisions required for equipartition between the wall and rotational temperatures through the relation $\zeta=e^{\ln\delta/Z}$, where δ is the desired closeness to equipartition (e.g., $\delta=0.1$ corresponds to an equiparition achievement of within 10%) and Z is the number of collisions required to attain this level of equipartition. Values of ζ for $\delta=10\%$, 5%, 1%, and 0.1% are shown in Table II. As can be seen from Table II, ζ values of ~0.2–0.4 should be used to achieve within 1% equipartition through several wall collisions. The characteristic rate for rotational level change due to wall collisions in the PFRC is thus 2–8 kHz. Note that the effects of wall temperature and gas temperature upon the rate are comparable for moderate to high temperatures (300–1000 K) and the effect of T_{wall} is more significant than T_{gas} at low temperatures (below ~300 K).

Recombination of hydrogen molecules from adsorbed H atoms at the walls can occur and is known to release molecules with a rotational energy distribution which is colder

TABLE II. Values of ζ needed to achieve equilibration within δ=0.1 to10% for various total number of collisions.

	δ (%)			
Number collisions Z	10	5	1	0.1
1	0.1	0.05	0.001	0.0001
2	0.32	0.22	0.1	0.03
3	0.46	0.37	0.22	0.1
4	0.56	0.47	0.32	0.18
5	0.63	0.55	0.40	0.25
6	0.68	0.61	0.46	0.32

than the wall temperature.[33–36] This "rotational cooling," caused by the sticking probability of hydrogen to the wall material decreasing with increasing N, could thus affect the overall rotational level populations within the PFRC chamber. The resulting colder distribution is also non-Boltzmann. However, an analysis was conducted which showed that the recombination rate is very small (<100 Hz) and therefore will be neglected in comparison with the other rates detailed above. Rotational cooling from wall recombination should be considered in other applications where recycling is a significant effect. This recombination analysis will be submitted for publication separately.

Resonant processes during electron-impact of H_2 molecules, such as dissociative attachment (DA), could potentially affect the rotational distribution.[37–41] In dissociative attachment, electron capture by H_2 forms an intermediate negative-ion state followed by dissociation and release of an electron, with higher rotational N states having higher probability of this occurring. Thus the rotational distribution could preferentially lose population from higher N levels, leading effectively to lower apparent rotational temperatures. However, resonant processes such as DA occur at low electron energies in hydrogen (<17 eV),[42] and the difference in DA cross sections for different rotational N states decreases rapidly beyond 5 eV. Also, the DA cross sections are not very large. For example, for the ground vibrational state (v=0) and N=8 the DA cross section is 10^{-20} cm^2,[37] such that a 5 eV electron energy with $n_e=10^{12}$ cm^{-3} results in an excitation rate of only ~1 Hz. Higher energies at ~100 eV would increase this rate only to ~4 Hz, if the cross section was to stay constant with energy (more likely decreasing), but again DA is not effective at altering the rotational distribution beyond 5–10 eV regardless. The DA cross sections decrease even further with lower N levels. Therefore, dissociative attachment will not be considered here, although it could be an important effect in some applications.

The total rate of change of the rotational populations is given by the sum of Eqs. (2), (5), (6a), (6b), and (7) as

$$\dot{n}_N^{\mathrm{tot}} = \dot{n}_N^{\mathrm{feed}}(\Gamma, T_{\mathrm{feed}}) + \dot{n}_N^{\mathrm{quad}}(n_N) + \dot{n}_N^{\Sigma\leftrightarrow\Sigma}(n_N) + \dot{n}_N^{\Sigma\leftrightarrow\Pi}(n_N) + \dot{n}_N^{\mathrm{wall}}(n_N, T_{\mathrm{wall}}, T_{\mathrm{gas}}). \quad (8)$$

In steady-state, $\dot{n}_N^{\mathrm{tot}}$ is set to zero in Eq. (8), and the rotational populations n_N are then obtained algebraically. However, the analytic solution of Eq. (8) is

$$n_N(t) = \frac{R_0}{\beta} + \left(n_N^0 - \frac{R_0}{\beta}\right)e^{-\beta t}, \quad (9)$$

where n_N^0 is the initial density of rotational level N, $\beta=(\zeta V_{H_2}/D)-(\dot{n}_N^{\mathrm{quad}}+\dot{n}_N^{\Sigma\leftrightarrow\Sigma}+\dot{n}_N^{\Sigma\leftrightarrow\Pi})/n_N$ and $R_0=(\dot{n}_N^{\mathrm{wall}}+(\zeta V_{H_2}/D)n_N)+\dot{n}_N^{\mathrm{feed}}$. Note that R_0 is the term in Eq. (7) containing the Boltzmann exponential factor plus the feed rate of Eq. (2). From Eq. (9) it is observed that the solution for n_N diverges for $\beta\leq 0$. Physically, this means that there is no steady-state solution when the nonequilibrating electron-impact rates overwhelm the equilibrating wall collision rate. A characteristic time to approach the steady-state solution of $n_N=R_0/\beta$ is the e-folding time $\tau=1/\beta$. The largest value of τ occurs for N=2, which is of the order of 0.1–0.4 ms. Since a PFRC plasma pulse is of duration of 2–3 ms, the steady-state solution is justified. However, this time scale also shows that measurements should be triggered to start at an appropriate time after τ.

III. RESULTS

The above equations were implemented into the numerical software package MATHEMATICA. The parameters Γ, ζ, T_{gas}, T_{wall}, and T_{feed} were adjusted to test the model. Nuclear spin degeneracy, which is 3 for odd N (*ortho*-modification) and 1 for even N (*para*-modification), is not included, but should be considered in modeling of spectral intensities. The plasma parameters typical of the PFRC were fixed at $n_e=10^{12}$ cm^{-3}, T_e=100 eV, and Γ=4 SCCM. Multiple combinations were studied and Fig. 3 provides a set of relevant examples where T_{feed} is fixed at 300 K, ζ=0.4, and the wall temperature is varied from 100 to 1000 K. The gas translational temperature will be somewhere between the feed gas and wall temperatures, and since its value is used only to calculate the wall collision rate, T_{gas} was arbitrarily set to the average of the wall temperature and feed gas temperature. T_{gas} was varied and produced very small changes to the sample results shown in Fig. 3.

As can be seen from Figs. 3(a) and 3(b), the N=0,1,2 levels follow approximately a Boltzmann distribution with temperatures higher than those of the higher rotational levels. The $N\geq 3$ levels in Figs. 3(a) and 3(b) also approximately follow Boltzmann distributions, but at temperatures between the wall and feed gas temperatures. For the T_{wall}=100 K case of Fig. 3(a), the model shows the distribution closely follows a Boltzmann distribution at the feed gas temperature of 300 K. This is due to the lower effectiveness of wall collisions at lower wall and gas temperatures in comparison with the gas feed rate. The T_{wall}=400 K case of Fig. 3(b) shows that wall and feed gas rates are approximately equal effects upon the rotational populations. The model for the T_{wall}=1000 K case of Fig. 3(c), however, shows a non-Boltzmann distribution, with enhanced population in the tails. This distribution shows that the wall is most effective at lower N at these temperatures and loses effectiveness at higher N as the gas feed rate becomes more important.

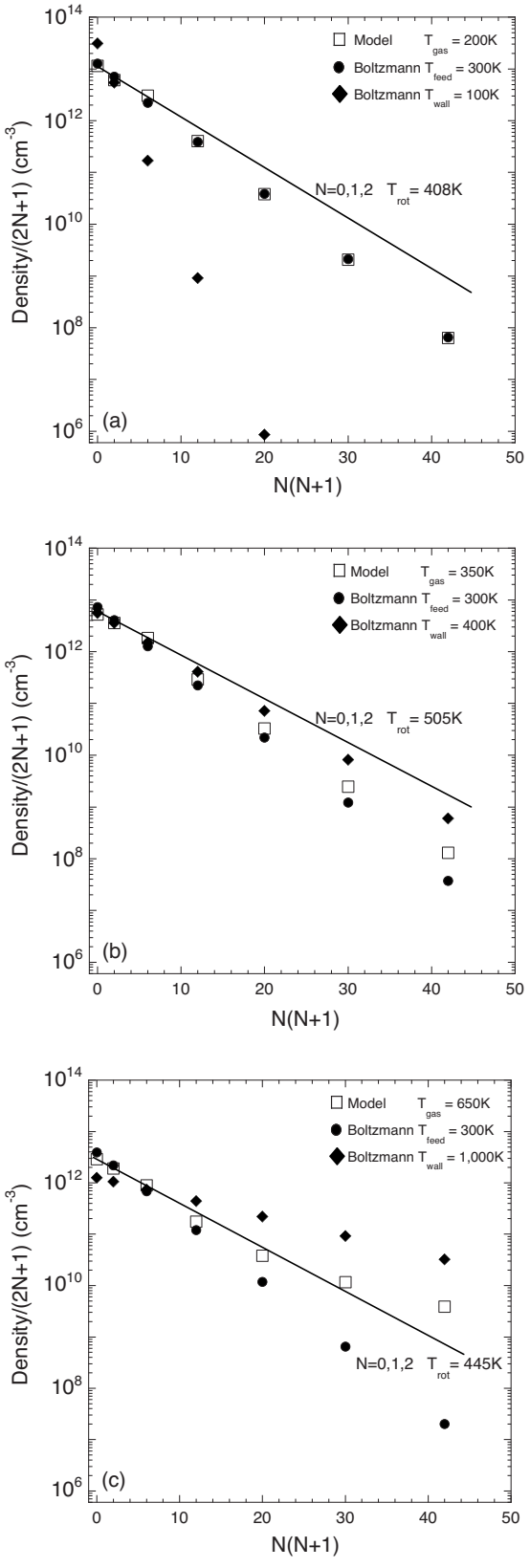

FIG. 3. Rotational level populations for the PFRC hydrogen gas confined within a 10 cm diameter vacuum chamber and ~7 cm flux conservers within which are $\sim 10^{12}$ cm^{-3} 100 eV electrons. The gas feed flow rate is $\Gamma=4$ SCCM to maintain a pressure of 1 mTorr, $\zeta=0.4$, and gas temperature is the average of the wall and feed gas temperature (set to 300 K). (a) $T_{wall}=100$ K, (b) $T_{wall}=400$ K, and (c) $T_{wall}=1000$ K.

The $N=0,1,2$ levels have the largest numerical factors in the brackets of Eqs. (5) and (6) for the quadrupole and dipole electron-impact rates, respectively, and these factors quickly decay for $N \geq 3$. Thus, electron-impact excitation is less effective at higher rotational levels, while equilibrating wall collisions and the feed gas addition can begin to dominate resulting in the higher rotational levels tending toward a Boltzmann distribution. At these higher rotational levels, the wall collision and feed gas effects compete to produce a steady-state Boltzmann distribution weighted toward the wall or feed gas temperature depending on their relative rates.

The model was also compared with the experimental results of Otorbaev *et al.*[5] [see Fig. 2(a) therein], which were obtained in a hydrogen discharge plasma at 0.5 Torr and current of 30 mA. An electron density of $\sim 10^{10}$ cm^{-3} at ~3 eV was reported separately by Lavrov *et al.*[9] Note that the data of Otorbaev *et al.* are from the fluorescent emission of the Fulcher-α system ($X\ ^1\Sigma_g^+ \leftarrow d\ ^3\Pi_u^- \rightarrow a\ ^3\Sigma_g^+$), so are representative of the upper N' rotational levels rather than the ground N levels. However, if dipole electron-impact excitation only is assumed (i.e., no quadrupole rovibronic excitation), then the upper levels are a direct mapping of the lower rotational levels since in this case only Q-branch excitation and emission transitions are possible ($\Delta N=0$). However, low-energy electron-impact excitation violates the first Born approximation, so quadrupole excitation may not be negligible. To correct the Otorbaev *et al.* upper rotational state intensities for direct comparison with the modeled ground state densities, their data were multiplied by the rotational constant ratio of the upper and ground electronic states B′/B, which is about 2 for the hydrogen Fulcher-α system.[14] Note that for the upper Π electronic state, $N'=0$ is not possible since $\Lambda=1$ in this case, which explains why no $N'=0$ point is shown for the Otorbaev *et al.* data of Fig. 4. All the population from the $N=0$ ground rotational level goes to the $d\ ^3\Pi_u^+$ $N'=1$ rovibronic parity state through a *R*-branch transition.

The electron-impact cross section for quadrupole excitation by electrons at ~3 eV is $\sim 10^{-16}$ cm^2.[27] These low electron energies are below the threshold for electron-impact excitation to upper electronic states, so the dipole electron-impact contributions detailed in Eq. (6) are neglected. The discharge tube was cooled with liquid nitrogen, so a wall temperature of 77 K is assumed in the model. No flux conservers were used. The gas temperature was obtained separately from Doppler broadening of H_2 spectral lines, giving a gas temperature estimate of 300 K. These plasma parameters were put into the model and the result is shown in Fig. 4. The model matches the experimental data of Otorbaev *et al.* quite well with a feed gas flow rate of 10 SCCM and $\zeta=0.4$. No flow rate was provided in their paper, but 10 SCCM is not unreasonable. However, it was found that an equivalent good fit with the Otorbaev *et al.* data is obtained with different combinations of ζ and Γ, as detailed in Table III. Interestingly, if the flow rate of the Otorbaev *et al.* experiment was known, then an experimental estimate of ζ could be obtained from matching the present model to their data.

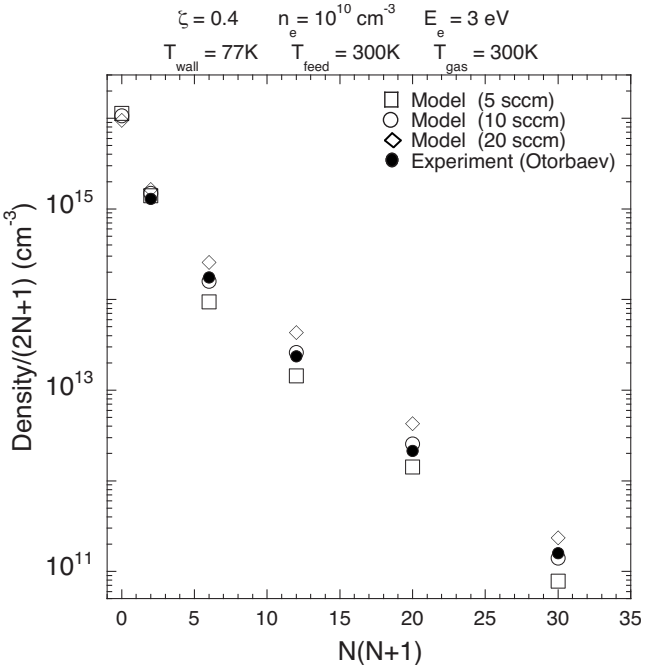

FIG. 4. Comparison of the experimental results of Otorbaev *et al.* (Ref. 5) with the model. Reported experimental parameters of T_{wall}=77 K, T_{gas} =300 K, and n_e=10^{10} cm^{-3} were used, and an electron energy of 3 eV inferred from the reported pressure and plasma current of the experiment. The feed gas flow rate was arbitrarily adjusted to 10 SCCM for ζ=0.4 to fit the experimental data, since no flow rate was given by Otorbaev *et al.* Equivalent fits were obtained using sets of ζ and Γ as shown in Table III.

IV. CONCLUSION

For medium-energy electrons (order 100 eV) at densities near the gas density, nonequilibrating quadrupole and dipole electron-impact excitations, given by Eqs. (5) and (6), respectively, can have a significant effect on the populations for low rotational levels (N=0,1,2) of ground state hydrogen. Low-energy electrons (less than threshold of ~15 eV) at densities near the gas density have a significant effect through quadrupole rovibrational excitation, but not dipole bound-electron transitions since they have very low probability of occurring at these energies. Under these conditions when the electron density is relatively high, the N=0,1,2 levels should not be considered in equilibrium with a rotational temperature obtained including higher rotational levels, unless the wall collision rate is large enough to overcome the nonequilibrating effect of the electron-impact excitation rates. For the case of the PFRC at the conditions expected, the N=0,1,2 levels follow a Boltzmann distribution at an effective rotational temperature higher than that would be obtained using all rotational levels. Since most of the molecular density is contained within the N=0,1,2 levels, a rotational temperature can be used to describe the distribution of the vast majority of molecules, but would not properly describe the populations of the higher N tails.

TABLE III. Feed gas flow rates Γ needed to match present model with data of Otorbaev *et al.* (Ref. 5) for various collision equilibration factors ζ.

ζ	0.2	0.3	0.4
Γ (SCCM)	4–5	7–8	9–10

It should be noted that *per* Eq. (9), the solution for the rotational level population diverges as the sum of the electron-impact rates approach the wall collision rate (i.e., as $\beta \rightarrow 0$). Small changes in the input plasma parameters in this regime result in large changes in the population distribution, especially for N=0,1,2, which may not be physical. However, this model clearly shows that the N=0,1,2 levels could have a distribution different from rest of the levels. Thus, it is not always justified to assume a Boltzmann distribution of the ground state rotational levels, in particular in studies of the Fulcher-α emission as a diagnostic for translational temperature.

The model was able to reproduce the non-Boltzmann rotational distribution reported by Otorbaev *et al.*[4,5] using their plasma parameters, except for the gas feed rate since no value was given. For this case, electron-impact excitation effects were smaller than wall collision and gas feed rate effects, although not completely negligible. It should be noted that much of the debate cited in the Introduction regarding the rotational distributions of hydrogen observed from Fulcher-α emissions did not fully consider the possible non-Boltzmann nature of the ground state molecules. Focus was instead placed on the mechanics of the electron-impact excitation process of the Fulcher-α system, leading for example to electron-impact excitation models with multipole transition moments.[4,16] For studies which did account for a non-Boltzmann initial distribution,[9] wall collisions and gas feed rate were not included, and to the author's knowledge no one has examined the effect of rovibronic electron-impact excitation processes as detailed in Fig. 2. Improper accounting of the ground rotational populations may therefore be the reason, at least in part, that multiple researchers have obtained non-Boltzmann rotational distributions from their Fulcher-α spectra, and thereby inappropriately derived a translational temperature from rotational spectra.

Recombination of molecular hydrogen at the walls and resonant processes, such as dissociative attachment, were found to be small effects for the PFRC. Additionally, dissociative attachment would be a small effect when applying the model to the data of Otorbaev *et al.* Intermolecular collisions should be included for other molecules beyond hydrogen and deuterium if their intermolecular collision rate, multiplied by the characteristic number collisions to equilibrate, is comparable with the other rates of Eq. (8).

ACKNOWLEDGMENTS

The author wishes to express his thanks and gratitude to Dr. Samuel Cohen for useful discussions. This work was supported, in part, by the U.S. Department of Energy Contract No. DE-AC02-76-CHO-3073.

[1] S. Chapman and T. G. Cowling, *The Mathematical Theory of Non-Uniform Gases* (Cambridge University Press, Cambridge, 1970), p. 246.
[2] T. L. Cottrell and J. C. McCoubrey, *Molecular Energy Transfer in Gases* (Butterworth, London, 1961), p. 78.
[3] H. Rabitz and S.-H. Lam, J. Chem. Phys. **63**, 3532 (1975).
[4] D. K. Otorbaev, V. N. Ochkin, P. L. Rubin, S. Yu. Savinov, N. N. Sobolev, and S. N. Tskhai, *Electron-Excited Molecules in Non-Equilibrium Plasmas*, edited by N. N. Sobolev (Nova Science Publishers, Commack, NY, 1985), pp. 121–173.

[5] D. K. Otorbaev, V. N. Ochkin, S. Yu. Savinov, N. N. Sobolev, and S. N. Tskhai, JETP Lett. **28**, 392 (1979).
[6] N. Ginsburg and G. H. Dieke, Phys. Rev. **59**, 632 (1941).
[7] M. J. de Graaf, Z. Qing, G. van Roojj, M. C. M. van de Sanden, R. M. A. Heeren, and A. W. Kleyn, AIP Conf. Proc. **287**, 588 (1994).
[8] B. P. Lavrov, V. N. Ostrovskii, and V. I. Ustimov, Opt. Spectrosc. **47**, 30 (1979).
[9] B. P. Lavrov, V. N. Ostrovskii, and V. I. Ustimov, Sov. Phys. Tech. Phys. **25**, 1208 (1980); **25**, 1213 (1980).
[10] B. P. Lavrov, A. A. Solov'ev, and M. V. Tyutchev, J. Appl. Spectrosc. **32**, 316 (1980).
[11] B. P. Lavrov, Opt. Spectrosc. **48**, 375 (1980).
[12] B. P. Lavrov, V. N. Ostrovskii, and V. I. Ustimov, Sov. Tech. Phys. Lett. **5**, 142 (1979).
[13] D. R. Welch, S. A. Cohen, T. C. Genoni, and A. H. Glasser, Phys. Rev. Lett. **105**, 015002 (2010).
[14] G. Herzberg, *Molecular Spectra and Molecular Structure* (Van Nostrand, New York, 1955).
[15] D. A. McQuarrie and J. D. Simon, *Molecular Thermodynamics* (University Science, Sausalito, CA, 1999), pp. 152–159.
[16] A. P. Bryukhovetskiy, E. N. Kotlikov, D. K. Otorbaev, V. N. Ochkin, P. L. Rubin, S. Yu. Savinov, and N. N. Sobolev, Sov. Phys. JETP **79**, 1687 (1980).
[17] R. Goldflam, D. J. Kouri, and S. Green, J. Chem. Phys. **67**, 5661 (1977).
[18] D. A. Varshalovich and V. K. Khersonskii, Sov. Phys. Tech. Phys. **26**, 901 (1981).
[19] N. F. Lane, Rev. Mod. Phys. **52**, 29 (1980).
[20] R. N. Zare, *Angular Momentum* (Wiley, New York, 1988), p. 63.
[21] J. D. Poll and L. Wolniewicz, J. Chem. Phys. **68**, 3053 (1978).
[22] P. K. Bhattacharyya and D. K. Syamal, Phys. Rev. A **30**, 126 (1984).
[23] G. Staszewska, D. W. Schwenke, and D. G. Truhlar, J. Chem. Phys. **81**, 335 (1984).
[24] A. Hansson and J. K. G. Watson, J. Mol. Spectrosc. **233**, 169 (2005).
[25] M. Born and R. Oppenheimer, Ann. Phys. **389**, 457 (1927); English version: Quantum Chemistry, Classic Scientific Papers, 1, 2000.
[26] U. Fantz and D. Wünderlich, At. Data Nucl. Data Tables **92**, 853 (2006).
[27] H. Tawara, Y. Itikawa, H. Nishimura, and M. Yoshino, J. Phys. Chem. Ref. Data **19**, 617 (1990).
[28] U. Fantz and B. Heger, Plasma Phys. Controlled Fusion **40**, 2023 (1998).
[29] D. Villarejo, R. Stockbauer, and M. G. Ingham, J. Chem. Phys. **50**, 1754 (1969).
[30] D.P. Lundberg and S.A. Cohen, Bull. Am. Phys. Soc. **51**, QO2.006 (2006).
[31] J.D. Huba, *NRL Plasma Formulary* (Naval Research Laboratory, Washington, DC, 2009), p. 29.
[32] A. M. Karo, J. R. Hiskes, K. D. Olwell, T. M. Deboni, and R. J. Hardy, AIP Conf. Proc. **111**, 197 (1984).
[33] H. Kasai and A. Okiji, Prog. Theor. Phys. Suppl. **106**, 341 (1991).
[34] K. W. Kolasinski, S. F. Shane, and R. N. Zare, J. Chem. Phys. **95**, 5482 (1991).
[35] S. F. Shane, K. W. Kolasinski, and R. N. Zare, J. Chem. Phys. **97**, 1520 (1992).
[36] W. A. Diño, H. Kasai, and A. Okiji, J. Phys. Soc. Jpn. **67**, 1517 (1998).
[37] I. I. Fabrikant, J. M. Wadehra, and Y. Xu, Phys. Scr. **T96**, 45 (2002).
[38] J. N. Bardsley and J. M. Wadehra, Phys. Rev. A **20**, 1398 (1979).
[39] J. M. Wadehra and J. N. Bardsley, Phys. Rev. Lett. **41**, 1795 (1978).
[40] J. M. Wadehra, Phys. Rev. A **29**, 106 (1984).
[41] J. P. Gauyacq, J. Phys. B **18**, 1859 (1985).
[42] M. Tronc, R. I. Hall, C. Schermann, and H. S. Taylor, J. Phys. B **12**, L279 (1979).